Article
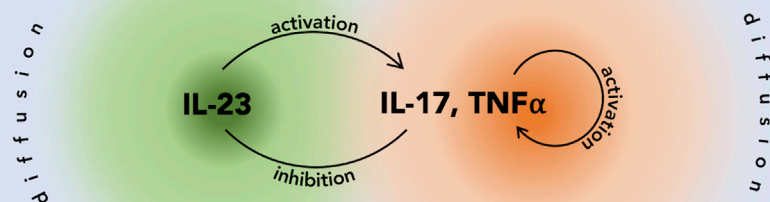
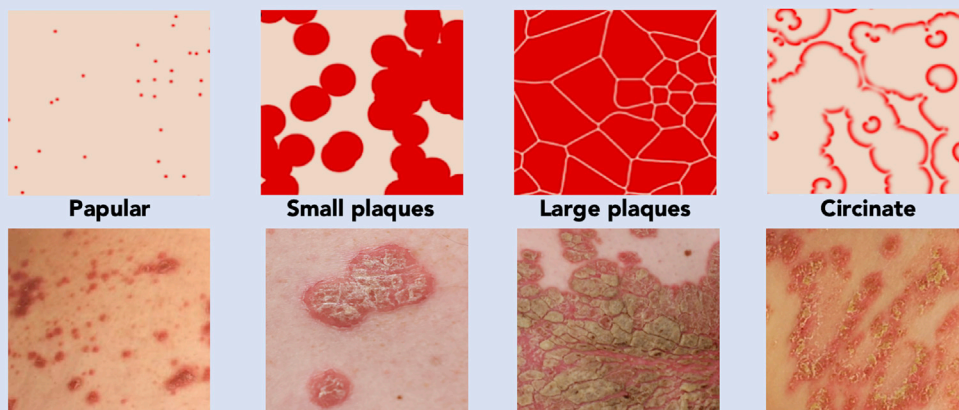# Skin Patterning in Psoriasis by Spatial Interactions between Pathogenic Cytokines

Mechanism of patterning in psoriasis

diffusion

activation

IL-23   IL-17, TNFα   activation

inhibition

diffusion

Computer modeling, reaction-diffusion

Patterns of inflammation matching human disease

Papular   Small plaques   Large plaques   Circinate

Lee Ringham,
Przemyslaw
Prusinkiewicz,
Robert Gniadecki

pwp@ucalgary.ca (P.P.)
r.gniadecki@ualberta.ca (R.G.)

HIGHLIGHTS
Skin lesions in psoriasis
are captured in reaction-
diffusion models (RDMs)

Activator-depleted
substrate RDM reflects
interactions of pathogenic
cytokines

Evolution of psoriatic
lesions is reproduced
using parameters from the
Gray-Scott space

Article

Skin Patterning in Psoriasis by Spatial Interactions between Pathogenic Cytokines

Lee Ringham,[1] Przemyslaw Prusinkiewicz,[1,4,*] and Robert Gniadecki[2,3,4,5,*]

SUMMARY

Disorders of human skin manifest themselves with patterns of lesions ranging from simple scattered spots to complex rings and spirals. These patterns are an essential characteristic of skin disease, yet the mechanisms through which they arise remain unknown. Here we show that all known patterns of psoriasis, a common inflammatory skin disease, can be explained in terms of reaction-diffusion. We constructed a computational model based on the known interactions between the main pathogenic cytokines: interleukins IL-17 and IL-23, and tumor necrosis factor TNF-α. Simulations revealed that the parameter space of the model contained all classes of psoriatic lesion patterns. They also faithfully reproduced the growth and evolution of the plaques and the response to treatment by cytokine targeting. Thus the pathogenesis of inflammatory diseases, such as psoriasis, may be readily understood in the framework of the stimulatory and inhibitory interactions between a few diffusing mediators.

INTRODUCTION

Most skin diseases manifest themselves with reproducible patterns of skin lesions, which are conventionally described in terms of lesion morphology (e.g., macules, papules, plaques) and distribution on the skin surface (Nast et al., 2016). The biological basis of pattern formation is only understood in a few special cases. For instance, the segmental pattern of herpes zoster reflects dermatomal viral reactivation through sensory nerves, and the linear pattern in Blaschko lines represents genetic mosaicism. In most cases, however, the mechanisms by which pathological processes in the skin generate reproducible patterns remain virtually unknown (Nast et al., 2016).

The majority of skin diseases are inflammatory, which explains why the lesions are often red, elevated, and scaly (resulting from, respectively, vasodilation and hyperemia, inflammatory infiltrate and edema, and pathologically increased epidermal keratinization secondary to inflammation). The skin has a large surface (average 1.5 m^2–2.0 m^2) compared with its thickness (0.5 mm–4 mm; surface-to-volume ratio of approximately 650m^2/m^3) (Leider, 1949) and is therefore ideally suited to study the mechanisms of the spatial propagation of inflammatory processes in a tissue. Psoriasis, a chronic, autoimmune inflammatory skin disease affecting 2%–3% of the population in Western countries (Parisi et al., 2013) provides a particularly useful model. The lesions are sharply demarcated, scaly, and distributed symmetrically on the body (Christophers, 2001; Griffiths and Barker, 2007; Nestle et al., 2009). The plaques evolve from pinpoint papules by centrifugal growth, which explains the oval contour of mature lesions (Farber et al., 1985; Soltani and Van Scott, 1972). Individual plaques may merge producing polycyclic contours (Christophers, 2001; Farber et al., 1985). In some instances the plaques have the appearance of rings (referred to as annular, arciform, or circinate patterns) (Christophers, 2001; Nast et al., 2016), which is the predominant morphological feature in approximately 5% patients (Morris et al., 2001). The mechanisms responsible for these patterns are not readily explainable in terms of the lateral propagation of inflammation, in which one would expect a gradual attenuation of inflammation due to the dilution of proinflammatory agents that diffuse in the skin. In contrast, in psoriatic lesions the intensity of inflammation is preserved throughout the whole plaque and sharply suppressed at its margin over the distance of a few millimeters. We show that the phenotypic features of psoriasis can be explained in terms of interactions between key pathogenic cytokines consistent with a reaction-diffusion model. This model captures all cardinal phenotypic features of psoriasis and may provide a wider framework to understand the patterning and maintenance of inflammation in other skin diseases.

RESULTS

Classification of Psoriasis Plaque Patterns

The patterns repetitively identified in the literature and in our clinical photograph repository are listed in Figure 1, with further morphological details characteristic of different patterns shown in Figure S1. As

[1]Department of Computer Science, University of Calgary, T2N 1N4 Calgary, Canada

[2]Division of Dermatology, Department of Medicine, University of Alberta, T6G 2G3 Edmonton, Canada

[3]Department of Dermatology, Bispebjerg Hospital, Bispebjerg Bakke 23, 2400 Copenhagen, Denmark

[4]Senior author

[5]Lead Contact

*Correspondence:
pwp@ucalgary.ca (P.P.),
r.gniadecki@ualberta.ca (R.G.)
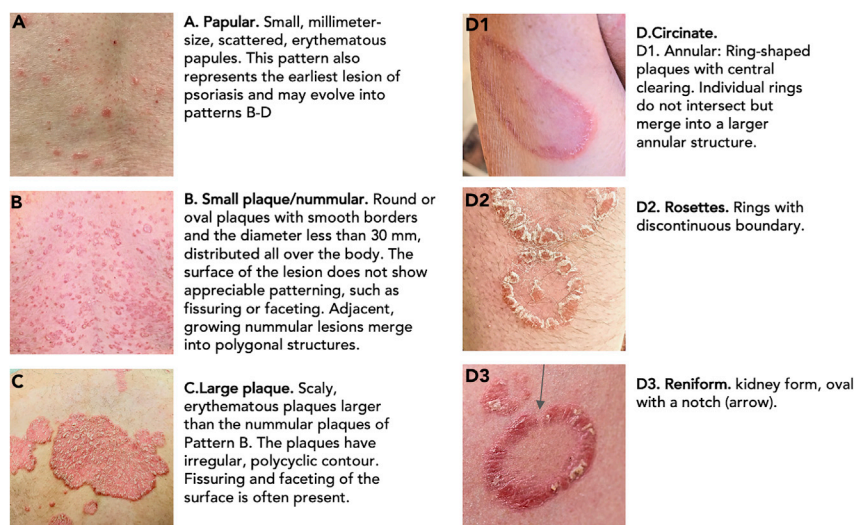
https://doi.org/10.1016/j.isci.
2019.10.008

Figure 1. Patterns of Skin Lesions in Psoriasis
See also Figure S1.

detailed in Transparent Methods, we have excluded linear psoriasis, psoriatic erythroderma, and guttate psoriasis from our classification.

A feature not explicitly discussed in the literature is the patterning of the plaque itself, manifest in the shape of the scales and/or irregularities of the plaque surface. The intensity of the inflammatory process is not homogeneous within the plaque. In the very early pinpoint papules the inflammatory infiltrate is most dense at the center, which translates into higher proliferative activity of the keratinocytes and a thicker scale centrally in the papule (Figure S1A) (Soltani and Van Scott, 1972). As the lesion grows the inflammatory infiltrate becomes more irregular, with a tendency toward higher activity at the periphery and occasional hotspots inside the plaque. A growing plaque, such as a nummular lesion, is thus often slightly thicker and scalier at the periphery than in the center. Likewise, the central portion of the plaque clears more rapidly during treatment, whereas the regression of inflammatory hotspots and the marginal region is delayed (Griffin et al., 1988). Large, mature plaques demonstrate a complex pattern of polygonal faceting rather than thickening of the margins (Figure S1D).

Model of Cytokine Interactions in Psoriasis

Cytokines interleukin IL-23, IL-17, and tumor necrosis factor TNF-α are central mediators in psoriatic plaque formation, as underscored by the fact that pharmacological blockade of either cytokine by monoclonal antibodies causes clinical remission in a large proportion of patients (Jabbar-Lopez et al., 2017). Interactions between the cytokines inferred from the available data are shown schematically in Figure 2A. The most important pathogenic cytokines are those of the IL-17 family, being produced primarily by T_H17 lymphocytes (interaction 0) (Krueger et al., 2012). These cells require IL-23 for expansion and activation (Cosmi et al., 2008; Wilson et al., 2007; Zheng et al., 2006) and amplify the inflammatory process by inducing other proinflammatory cytokines, the most important of which is TNF-α (Boehncke and Schön, 2015). Psoriatic plaques contain both dendritic cells producing IL-23 and T_H17 cells expressing the IL-23 receptor (Cosmi et al., 2008; Lee et al., 2004; Tillack et al., 2014; Wilson et al., 2007). Treatment with guselkumab, a selective therapeutic monoclonal antibody inhibiting IL-23, attenuates IL-17s in psoriatic plaques and in serum in patients with psoriasis (interaction 1) (Hawkes et al., 2018; Sofen et al., 2014; Tillack et al., 2014). This attenuation is correlated with the clinical clearing of psoriasis lesions (Sofen et al., 2014). IL-17 and TNF-α synergize with each other (Alzabin et al., 2012; Krueger et al., 2012; Xu et al., 2017): IL-17 increases the expression of TNF-α (Jovanovic et al., 1998) (interaction 2), whereas therapeutic TNF-α inhibition blocks IL-17 in responding patients (interaction 3) (Zaba et al., 2007, 2009). The positive feedback of IL-17 cytokines on their own production (interactions 2 and 3) is further demonstrated by the findings that IL-17A induces IL-17C (Xu et al., 2018) and that the therapeutic inhibition of the IL-17 receptor with brodalumab reduces the expression of the IL-17 cytokine (IL-17A, C, F) (Russell et al., 2014). TNF-α downregulates IL-23 (interaction 4) either directly (Notley et al., 2008; Zakharova and Ziegler, 2005) or indirectly via the inhibition of
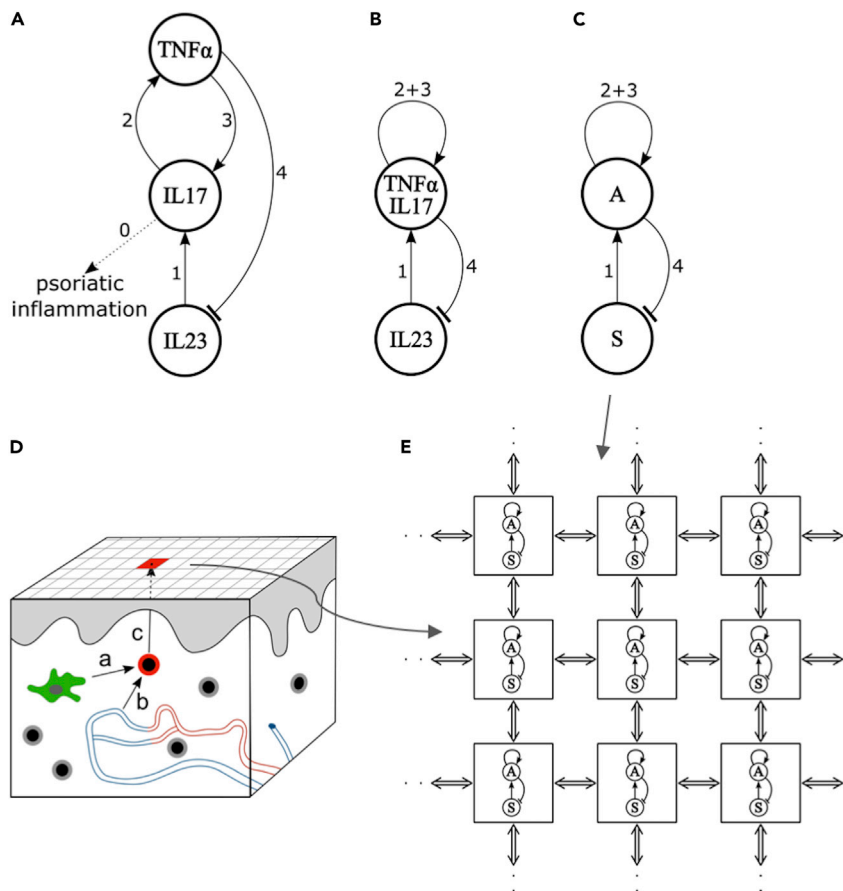
Figure 2. Modeling Plaque Formation in Psoriasis

(A) Interactions between key cytokines involved in psoriasis plaque formation. Labels numbered 0–4 refer to the observations from which these interactions have been inferred (see Results).

(B) A simplified diagram of interactions, in which cytokines IL-17 and TNF-α are considered jointly.

(C) Diagram (B) relabeled as an activator (A) - depleted substrate (S) system.

(D) Skin representation and simulation initialization. The skin surface is partitioned into square regions. A lesion is initiated by an activated T_H17 cell (red), which is either a resident memory T cell activated by a dendritic cell (green, interaction **a**) or has migrated from circulation through a capillary wall (interaction **b**). The area of microinflammation around the activated T_H17 cell is considered as a "seed" region, and its projection to the surface (arrow **c**) is colored in red. The epidermis, the upper layer of the skin, is shaded in gray and capillaries in the dermis are colored in red (arterioles) and blue (venules). Skin-resident memory T cells are marked in gray.

(E) Detail of skin surface representation. Each region is a two-dimensional projection of the underlying activator-depleted substrate system of proinflammatory cytokines and represents a computational cell implementing reaction system (C). These computational cells are interconnected (double arrows), allowing for the diffusion of cytokines.

interferons (Palucka et al., 2005; Tillack et al., 2014). Disturbance of this negative interaction is probably responsible for paradoxical induction of psoriasis in patients with rheumatoid arthritis and inflammatory bowel disease treated with TNF-α antibodies (Palucka et al., 2005; Tillack et al., 2014). This induction is readily reverted by therapeutic inhibition of the excess of IL-23 by ustekinumab, an antibody binding to the p40 chain of IL-23 (Tillack et al., 2014).

Computational Model Construction

To analyze whether the molecular-level interactions depicted in Figure 2A can account for the observed plaque patterns and the response of the disease to treatment, we constructed a mathematical model. We followed the standard method of simplifying the modeled system to focus on its essence and make it more amenable to analysis (Bak, 1996; Gaines, 1977; Prusinkiewicz, 1998). This simplification reduced the size of the parameter space and thus, to the extent possible, the use of parameters for which

quantitative data are currently unavailable. It has also related the problem of plaque pattern formation to a known class of reaction-diffusion systems, which provided guidance for the exploration of the parameter space, and facilitated the analysis and interpretation of the results.

We have pursued the following train of thought. The mutual promotion of cytokines IL-17 and TNF-α, represented by interactions **2** and **3** in Figure 2A, suggests that their concentrations may change in concert. Assuming this is the case, we reduced the three-substance graph in Figure 2A by representing IL-17 and TNF-α jointly. The resulting two-substance graph (Figure 2B) has the structure of an activator-depleted substrate reaction-diffusion model (Gierer and Meinhardt, 1972; Marcon et al., 2016) (Figure 2C). In this model, the substrate S with concentration s is locally converted into the activator A with concentration a according to the canonical equations (Gierer and Meinhardt, 1972; Meinhardt, 1982):

$$\frac{\partial a}{\partial t} = ka^2s + \rho_{a0} - \mu_a a + D_a \nabla^2 a,$$
$$\frac{\partial s}{\partial t} = -ka^2s + \rho_{s0} - \mu_s s + D_s \nabla^2 s. \qquad \text{(Equation 1)}$$

The term ka^2s indicates that the conversion is autocatalytically promoted by the activator, with the rate controlled by parameter k. The activator concentration increases at the expense of the substrate, thus the activator downregulates the substrate. Parameters ρ_{a0} and ρ_{s0} are the rates of the base production of the activator and the substrate, and μ_a and μ_s control their turnover. The remaining terms, $D_a \nabla^2 a$ and $D_s \nabla^2 s$, represent diffusion of the activator and substrate at rates controlled by parameters D_a and D_s, respectively (for simplicity, diffusion is not explicitly represented in Figures 2A–2C). Consistent with Figures 2B and 2C, we identify variable a with the concentration of cytokines TNF-α and IL-17 and s with the concentration of IL-23:

$$a = [TNF\alpha, IL17], \quad s = [IL23].$$

In the simulations, a patch of skin surface (Figure 2D) is represented by an array of interconnected computational "cells," each of which performs local computation according to Equation 1 (Figure 2E). The initial state in all simulations is a uniform distribution of IL-23 in the whole array, except for randomly distributed small "seed" areas with a high concentration of IL-17 and TNF-α. These areas represent IL-17-secreting cells (such as the T_H17-cell) that either have been activated *in situ* (Figure 2D, interaction **a**) or have migrated from the circulation to the skin (Figure 2D, interaction **b**) (Krueger et al., 2012).

Exploration of the Model Parameter Space

Currently it is not feasible to measure the diffusion of cytokines in human skin, hence there are no experimental data to provide suggestions for the parameter values of the model. Consequently, we adopted a reverse strategy, where we explored the model parameter space by searching for values that would yield psoriasis patterns observed in patients (Figure 1). To guide this search, we referred to the Gray-Scott reaction-diffusion system (Gray and Scott, 1984), for which the parameter space has been thoroughly explored:

$$\frac{\partial a}{\partial t} = a^2s - (f + c)a + D_a \nabla^2 a$$
$$\frac{\partial s}{\partial t} = -a^2s + (1 - s)f + D_s \nabla^2 s \qquad \text{(Equation 2)}$$

We observe (see also Yamamoto and Miorandi, 2010; Yamamoto et al., 2011) that Equation 2 are a special case of Equation 1, where

$$k = 1, \quad \rho_{a0} = 0, \quad \mu_a = f + c, \quad \rho_{s0} = f, \quad \mu_s = f.$$

The parameter space and details of six patterns obtained for specific parameter values are shown in Figure 3. These patterns correspond visually to the six types of psoriasis identified in patients (Figure 1). Note that, consistent with the common assumption of the Gray-Scott reaction-diffusion model, the ratio of the diffusion rates of substrate and activator was set to $D_s:D_a = 2$ (Pearson, 1993). This is a departure from the much larger ratios typically used in reaction-diffusion models (Diego et al., 2018; Gierer and Meinhardt, 1972; Kondo and Miura, 2010; Lengyel and Epstein, 1991; Marcon et al., 2016; Vastano et al., 1987). On biochemical grounds, this departure is justified by the commensurate small size of the three cytokines, implying comparable diffusion rates (see Table S1). The small ratio of diffusion rates does not preclude Turing instability and spontaneous pattern emergence for carefully chosen values of
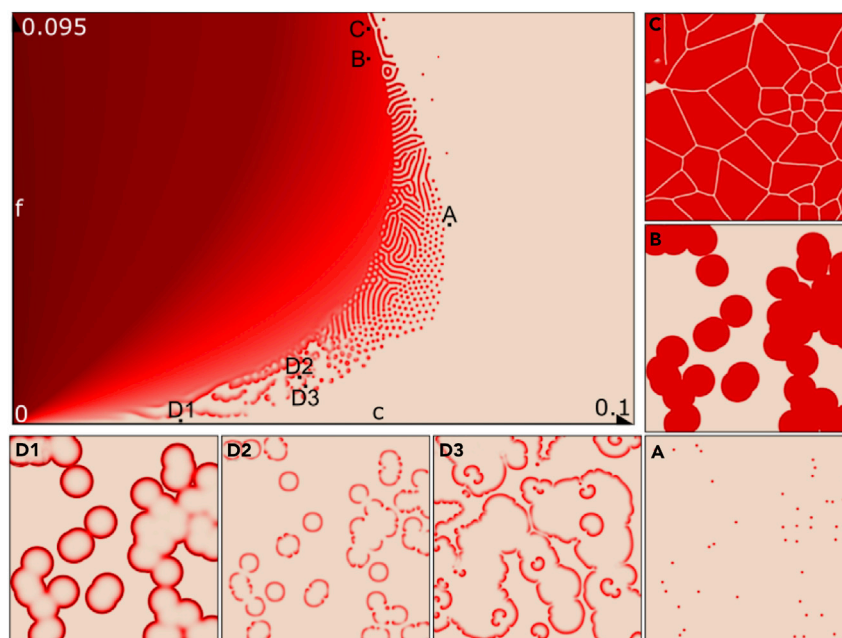
Figure 3. Parameter Space of the Model and Selected Patterns

Top left: A comprehensive representation of the range of patterns generated using Equation 2 for different values of the synthetic parameters *c* and *f*.

(A–D) Magnified views of patterns generated using select parameter values. These labels and patterns correspond to the psoriatic skin lesions identified in Figure 1.

the remaining parameters (see Figure S2). Nevertheless, the parameter values leading to the formation of plaque patterns are compatible with the "filtering" operation mode, in which the patterns do not emerge spontaneously in a homogeneous medium and elaborate the initial pre-patterns instead (Diego et al., 2018; Lee et al., 1993; Muratov and Osipov, 2000; Pearson, 1993). This latter mode is more pertinent to the development of psoriasis plaques, which is initiated by activated T_H17 cells in the skin (Figure 2D).

The Development of Lesions and Response to Treatment

The simulated development of psoriasis lesions and the response to treatment are shown in Figure 4 and in Videos S1, S2, S3, S4, S5, and S6. The development was simulated by using the forward Euler method to advance the state of the reaction-diffusion model over time, given an initial random distribution of small papules. The parameter values and initial conditions for each of these simulations are listed in Table S2, with additional information characterizing the sensitivity of simulations to the variation of (individual) parameter values collected in Table S3. Minimum values of the activator A, representing cytokines IL-17 and TNF-α, needed to initiate pattern formation are given in Table S4. The simulated patterns shown in Figure 4 have a striking resemblance to the actual patterns of psoriatic skin lesions shown in Figure 1. Next, we simulated the effect of therapy by increasing the decay rate of cytokines IL-17 and TNF-α (activator A), which mimics real-life treatment with an anti-cytokine antibody. Interestingly, the simulated lesion clearing was not simply a time reversal of the processes of plaque formation: the interior of the plaques cleared first, producing annular lesions (Figure 4, row 5). The residual lesions dispersed slowly, eventually disappearing entirely or leaving residual spots (Figure 4, row 6). These results closely resemble clinical situations, in which residual annular or papular lesions are often observed (Figure S1C).

Finally, to verify that the modeling results do not critically depend on the reduction of the three-substance system in Figure 2A to the two-substance system in Figure 2B, we have constructed a simulation model corresponding directly to Figure 2A (see Supplemental Equations). Guided in part by parameter values found for the two-substance model (Tables S2 and S3), we found values for which the three-substance model produces qualitatively the same plaque patterns (Table S5). This result validates the simplification underlying the two-substance model.
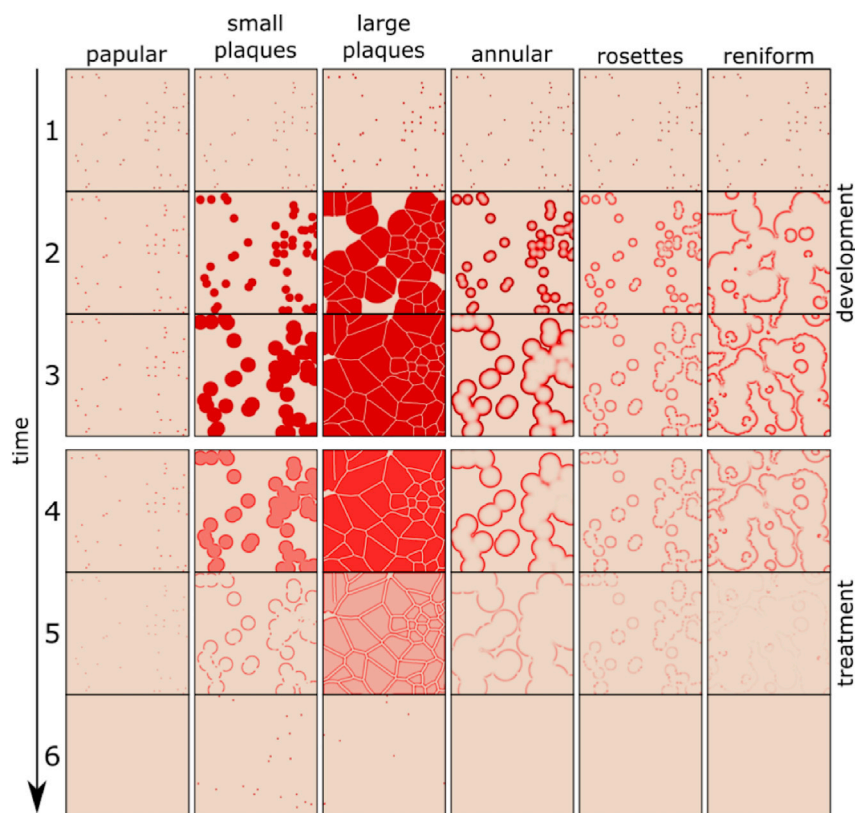
Figure 4. The Simulated Progression of Different Types of Psoriatic Lesions

Rows 1–3: Development of the lesions. The earliest stage of a papule (Row 1) consists of randomly distributed small seed areas. Later forms of the disease (Rows 2 and 3) correspond to patterns identified in Figures 1 and 3. Rows 4–6: The effect of treatment simulated by increasing the decay rate of IL-17 and TNF-α. Note that the treatment does not result in a simple reversal of the original pattern development, but produces residual lesions with more activity at the margin of the plaques (Row 5). In some instances, residual papules persist (Row 6).

DISCUSSION

Since the foundation of dermatology as a medical specialty in the beginning of the 19th century, morphological patterns provided a useful and robust criterion for the diagnosis and classification of skin diseases. However, the mechanisms by which skin diseases produce diverse patterns remained unknown. We have shown that all major morphological types of the common skin disease psoriasis (papular, small plaque, large plaque, and different forms of circinate patterns) can be generated by a reaction-diffusion model with different parameter values. The model is based on the currently known up- and down-regulating interactions between three proinflammatory cytokines: TNF-α, IL-23, and IL-17. These interactions are not direct chemical reactions, but are mediated by immunologically active cells stimulating or inhibiting the release and proliferation of intermediary cytokines. The model has a spatiotemporal character, explaining the emergence of patterns during disease development and their disappearance during subsequent treatment. Reaction-diffusion thus provides a promising framework for studying mechanisms underlying the progress and treatment of psoriasis. As detailed data regarding the interaction and diffusion of cytokines involved in psoriasis become available, more elaborate models may be constructed to re-create the actual biological processes in the skin with increased accuracy. Recent advances in the theoretical understanding of reaction-diffusion (Diego et al., 2018) suggest that the resulting models may also become more robust to parameter changes, currently limited to narrow ranges.

Inflammatory patterns related to psoriasis are found in other diseases as well. For example, annular lesions are seen in erythema multiforme, dermatophytosis, and erythema annulare centrifugum; reniform patterns in erythema gyratum repens, urticaria, and lupus erythematosus; and rosettes in granuloma annulare. We

thus hypothesize that reaction-diffusion models can be applied further to explain the patterns of other inflammatory skin diseases and suggest their treatment by selective cytokine inhibition. Eventually, reaction-diffusion models could provide a framework for understanding the pathogenesis and pharmacologic intervention of a broad spectrum of skin diseases.

Limitations of the Study

The model is based on qualitative results describing the interaction of cytokines in the skin, but its predictions have not yet been confirmed by measurements of cytokine concentrations and propagation rates in the skin. Such measurements are currently difficult for a combination of technical and ethical reasons and thus are left as a topic for further research, which we hope our work will motivate.

METHODS

All methods can be found in the accompanying Transparent Methods supplemental file.

SUPPLEMENTAL INFORMATION

Supplemental Information can be found online at https://doi.org/10.1016/j.isci.2019.10.008.

AUTHOR CONTRIBUTIONS

P.P. and R.G. designed research; L.R. and P.P. created the mathematical model and performed computer simulations; L.R., P.P. and R.G. wrote the paper.

DECLARATION OF INTERESTS

L.R., P.P., and R.G. have no conflict to declare.

REFERENCES

Alzabin, S., Abraham, S.M., Taher, T.E., Palfreeman, A., Hull, D., McNamee, K., Jawad, A., Pathan, E., Kinderlerer, A., Taylor, P.C., et al. (2012). Incomplete response of inflammatory arthritis to TNFα blockade is associated with the Th17 pathway. Ann. Rheum. Dis. 71, 1741–1748.

Bak, P. (1996). How Nature Works. The Science of Self-Organized Criticality (Springer).

Boehncke, W.-H., and Schön, M.P. (2015). Psoriasis. Lancet 386, 983–994.

Christophers, E. (2001). Psoriasis–epidemiology and clinical spectrum. Clin. Exp. Dermatol. 26, 314–320.

Cosmi, L., De Palma, R., Santarlasci, V., Maggi, L., Capone, M., Frosali, F., Rodolico, G., Querci, V., Abbate, G., Angeli, R., et al. (2008). Human interleukin 17-producing cells originate from a CD161+CD4+ T cell precursor. J. Exp. Med. 205, 1903–1916.

Diego, X., Marcon, L., Müller, P., and Sharpe, J. (2018). Key features of turing systems are determined purely by network topology. Phys. Rev. X 8, https://doi.org/10.1103/physrevx.8.021071.

Farber, E.M., Nall, L., and Strefling, A. (1985). Psoriasis: a disease of the total skin. J. Am. Acad. Dermatol. 12, 150–156.

Gaines, B.R. (1977). System identification, approximation and complexity. Int. J. Gen. Syst. 3, 145–174.

Gierer, A., and Meinhardt, H. (1972). A theory of biological pattern formation. Kybernetik 12, 30–39.

Gray, P., and Scott, S.K. (1984). Autocatalytic reactions in the isothermal, continuous stirred tank reactor. Chem. Eng. Sci. 39, 1087–1097.

Griffin, T.D., Lattanand, A., and VanScott, E.J. (1988). Clinical and histologic heterogeneity of

psoriatic plaques. Therapeutic relevance. Arch. Dermatol. 124, 216–220.

Griffiths, C.E., and Barker, J.N. (2007). Pathogenesis and clinical features of psoriasis. Lancet 370, 263–271.

Hawkes, J.E., Yan, B.Y., Chan, T.C., and Krueger, J.G. (2018). Discovery of the IL-23/IL-17 signaling pathway and the treatment of psoriasis. J. Immunol. 201, 1605–1613.

Jabbar-Lopez, Z.K., Yiu, Z.Z.N., Ward, V., Exton, L.S., Mohd Mustapa, M.F., Samarasekera, E., Burden, A.D., Murphy, R., Owen, C.M., Parslew, R., et al. (2017). Quantitative evaluation of biologic therapy options for psoriasis: a systematic review and network meta-analysis. J. Invest. Dermatol. 137, 1646–1654.

Jovanovic, D.V., Di Battista, J.A., Martel-Pelletier, J., Jolicoeur, F.C., He, Y., Zhang, M., Mineau, F., and Pelletier, J.P. (1998). IL-17 stimulates the production and expression of proinflammatory

cytokines, IL-beta and TNF-alpha, by human macrophages. J. Immunol. *160*, 3513–3521.

Kondo, S., and Miura, T. (2010). Reaction-diffusion model as a framework for understanding biological pattern formation. Science *329*, 1616–1620.

Krueger, J.G., Fretzin, S., Suárez-Fariñas, M., Haslett, P.A., Phipps, K.M., Cameron, G.S., McColm, J., Katcherian, A., Cueto, I., White, T., et al. (2012). IL-17A is essential for cell activation and inflammatory gene circuits in subjects with psoriasis. J. Allergy Clin. Immunol. *130*, 145–154.e9.

Lee, K.J., McCormick, W.D., Ouyang, Q., and Swinney, H.L. (1993). Pattern formation by interacting chemical fronts. Science *261*, 192–194.

Lee, E., Trepicchio, W.L., Oestreicher, J.L., Pittman, D., Wang, F., Chamian, F., Dhodapkar, M., and Krueger, J.G. (2004). Increased expression of interleukin 23 p19 and p40 in lesional skin of patients with psoriasis vulgaris. J. Exp. Med. *199*, 125–130.

Leider, M. (1949). On the weight of the skin. J. Invest. Dermatol. *12*, 187–191.

Lengyel, I., and Epstein, I.R. (1991). Modeling of turing structures in the chlorite–iodide–malonic Acid–starch reaction system. Science *251*, 650–652.

Marcon, L., Diego, X., Sharpe, J., and Müller, P. (2016). High-throughput mathematical analysis identifies Turing networks for patterning with equally diffusing signals. Elife *5*, https://doi.org/10.7554/eLife.14022.

Meinhardt, H. (1982). Models of Biological Pattern Formation (Academic Press).

Morris, A., Rogers, M., Fischer, G., and Williams, K. (2001). Childhood psoriasis: a clinical review of 1262 cases. Pediatr. Dermatol. *18*, 188–198.

Muratov, C.B., and Osipov, V.V. (2000). Static spike autosolitons in the Gray-Scott model. J. Phys. A Math. Gen. *33*, 8893–8916.

Nast, A., Griffiths, C.E.M., Hay, R., Sterry, W., and Bolognia, J.L. (2016). The 2016 International League of Dermatological Societies' revised glossary for the description of cutaneous lesions. Br. J. Dermatol. *174*, 1351–1358.

Nestle, F.O., Kaplan, D.H., and Barker, J. (2009). Psoriasis. N. Engl. J. Med. *361*, 496–509.

Notley, C.A., Inglis, J.J., Alzabin, S., McCann, F.E., McNamee, K.E., and Williams, R.O. (2008).

Blockade of tumor necrosis factor in collagen-induced arthritis reveals a novel immunoregulatory pathway for Th1 and Th17 cells. J. Exp. Med. *205*, 2491–2497.

Palucka, A.K., Blanck, J.-P., Bennett, L., Pascual, V., and Banchereau, J. (2005). Cross-regulation of TNF and IFN-alpha in autoimmune diseases. Proc. Natl. Acad. Sci. U S A *102*, 3372–3377.

Parisi, R., Symmons, D.P.M., Griffiths, C.E.M., and Ashcroft, D.M.; Identification and Management of Psoriasis and Associated ComorbidiTy (IMPACT) Project Team (2013). Global epidemiology of psoriasis: a systematic review of incidence and prevalence. J. Invest. Dermatol. *133*, 377–385.

Pearson, J.E. (1993). Complex patterns in a simple system. Science *261*, 189–192.

Prusinkiewicz, P. (1998). In search of the right abstraction: the synergy between art, science, and information technology in the modeling of natural phenomena. In Art @ Science, C. Sommerer and L. Mignonneau, eds. (Springer), pp. 60–68.

Russell, C.B., Rand, H., Bigler, J., Kerkof, K., Timour, M., Bautista, E., Krueger, J.G., Salinger, D.H., Welcher, A.A., and Martin, D.A. (2014). Gene expression profiles normalized in psoriatic skin by treatment with brodalumab, a human anti-IL-17 receptor monoclonal antibody. J. Immunol. *192*, 3828–3836.

Sofen, H., Smith, S., Matheson, R.T., Leonardi, C.L., Calderon, C., Brodmerkel, C., Li, K., Campbell, K., Marciniak, S.J., Jr., Wasfi, Y., et al. (2014). Guselkumab (an IL-23-specific mAb) demonstrates clinical and molecular response in patients with moderate-to-severe psoriasis. J. Allergy Clin. Immunol. *133*, 1032–1040.

Soltani, K., and Van Scott, E.J. (1972). Patterns and sequence of tissue changes in incipient and evolving lesions of psoriasis. Arch. Dermatol. *106*, 484–490.

Tillack, C., Ehmann, L.M., Friedrich, M., Laubender, R.P., Papay, P., Vogelsang, H., Stallhofer, J., Beigel, F., Bedynek, A., Wetzke, M., et al. (2014). Anti-TNF antibody-induced psoriasiform skin lesions in patients with inflammatory bowel disease are characterised by interferon-γ-expressing Th1 cells and IL-17A/IL-22-expressing Th17 cells and respond to anti-IL-12/IL-23 antibody treatment. Gut *63*, 567–577.

Vastano, J.A., Pearson, J.E., Horsthemke, W., and Swinney, H.L. (1987). Chemical pattern formation with equal diffusion coefficients. Phys. Lett. A *124*, 320–324.

Wilson, N.J., Boniface, K., Chan, J.R., McKenzie, B.S., Blumenschein, W.M., Mattson, J.D., Basham, B., Smith, K., Chen, T., Morel, F., et al. (2007). Development, cytokine profile and function of human interleukin 17-producing helper T cells. Nat. Immunol. *8*, 950–957.

Xu, T., Ying, T., Wang, L., Zhang, X.D., Wang, Y., Kang, L., Huang, T., Cheng, L., Wang, L., and Zhao, Q. (2017). A native-like bispecific antibody suppresses the inflammatory cytokine response by simultaneously neutralizing tumor necrosis factor-alpha and interleukin-17A. Oncotarget *8*, 81860–81872.

Xu, M., Lu, H., Lee, Y.-H., Wu, Y., Liu, K., Shi, Y., An, H., Zhang, J., Wang, X., Lai, Y., et al. (2018). An interleukin-25-mediated autoregulatory circuit in keratinocytes plays a pivotal role in psoriatic skin inflammation. Immunity *48*, 787–798.e4.

Yamamoto, L., and Miorandi, D. (2010). Evaluating the robustness of activator-inhibitor models for cluster head computation. In Lecture Notes in Computer Science, pp. 143–154.

Yamamoto, L., Miorandi, D., Collet, P., and Banzhaf, W. (2011). Recovery properties of distributed cluster head election using reaction–diffusion. Swarm Intelligence *5*, 225–255.

Zaba, L.C., Cardinale, I., Gilleaudeau, P., Sullivan-Whalen, M., Suárez-Fariñas, M., Fuentes-Duculan, J., Novitskaya, I., Khatcherian, A., Bluth, M.J., Lowes, M.A., et al. (2007). Amelioration of epidermal hyperplasia by TNF inhibition is associated with reduced Th17 responses. J. Exp. Med. *204*, 3183–3194.

Zaba, L.C., Suárez-Fariñas, M., Fuentes-Duculan, J., Nograles, K.E., Guttman-Yassky, E., Cardinale, I., Lowes, M.A., and Krueger, J.G. (2009). Effective treatment of psoriasis with etanercept is linked to suppression of IL-17 signaling, not immediate response TNF genes. J. Allergy Clin. Immunol. *124*, 1022–1110.e1–e395.

Zakharova, M., and Ziegler, H.K. (2005). Paradoxical anti-inflammatory actions of TNF-alpha: inhibition of IL-12 and IL-23 via TNF receptor 1 in macrophages and dendritic cells. J. Immunol. *175*, 5024–5033.

Zheng, Y., Danilenko, D.M., Valdez, P., Kasman, I., Eastham-Anderson, J., Wu, J., and Ouyang, W. (2006). Interleukin-22, a TH17 cytokine, mediates IL-23-induced dermal inflammation and acanthosis. Nature *445*, 648–651.

Supplemental Information

Skin Patterning in Psoriasis by Spatial

Interactions between Pathogenic Cytokines

Lee Ringham, Przemyslaw Prusinkiewicz, and Robert Gniadecki

Transparent Methods

Source of information on the patterns of psoriatic lesions

Patterns of skin lesions in psoriasis have been reviewed using the "(psoriasis AND clinical AND (pattern OR shapes)) OR (clinical spectrum AND psoriasis)" search phrases in PubMed. We retrieved 715 papers and after reviewing the titles and abstracts we selected 40 relevant papers (Ayala, 2007; Baker, 1971; Balato et al., 2009; Beylot et al., 1979; Buxton, 1987; Champion, 1986; Chau et al., 2017; Christophers, 2001; Cordoro, 2008; Di Meglio et al., 2014; Fernandes et al., 2011; Gropper, 2001; Hernández-Vásquez et al., 2017; Hodge and Comaish, 1977; Jablonska et al., 2000; Kumar et al., 1995; Lal, 1966; Lebwohl, 2003; Magro and Crowson, 1997; Meier and Sheth, 2009; Melski et al., 1983; Menter and Barker, 1991; M G et al., 2013; Mitchell, 1962; Morris et al., 2001; Naldi and Gambini, 2007; de Oliveira et al., 2010; Picciani et al., 2017; Rasmussen, 1986; Raychaudhuri et al., 2014; Reich et al., 2009; Saleh and Tanner, 2018; Schön et al., 2005; Seneschal et al., 2012; Stankier, 1974; Stern, 1997; Talwar et al., 1995; Whyte and Baughman, 1964; Wollenberg and Eames, 2011; Ziemer et al., 2009). We also reviewed 482 clinical photographs of psoriasis in the database of the Department of Dermatology, University of Copenhagen and the Division of Dermatology, University of Alberta. We have excluded linear psoriasis, psoriatic erythroderma, and guttate psoriasis from our analyses. The linear pattern is the isomorphic (Köbner) response to trauma and does not emerge spontaneously (Melski et al., 1983). Erythroderma manifests itself as diffuse redness and inflammation of the entire skin, and thus lacks features of a pattern. Guttate psoriasis is considered to be a separate clinical type of the disease (Rasmussen, 1986; Raychaudhuri et al., 2014; Whyte and Baughman, 1964), but it is not distinguishable from papular or nummular psoriasis based on lesion morphology.

Computer model

The progress and treatment of the disease was simulated by numerically solving the initial value problem for the reaction-diffusion equations using the forward Euler method. Simulations have been implemented using a custom reaction-diffusion modeling program written in C++ within the Windows Visual Studio programming environment. To facilitate interactive exploration of the models and their parameters, computation has been accelerated (carried out in a parallel fashion) on a Nvidia GeForce GTX 850M Graphical Processing Unit, with arrays representing the previous and current state of the simulation in each step implemented as textures (Dematté and Prandi, 2010; Harris et al., 2005). The textures used in all simulations had a resolution of 500 x 500 texels, with each texel representing a sample point of a discretized patch of the skin. Parameters of individual simulations are collected in Table S1. We assumed Neumann boundary conditions set to 0, i.e., no diffusion of activator A and substrate S across the boundary. The initial activator concentration a was set to 0 in each texel except for 50 seed spots, placed randomly across the domain. Each spot was represented by a 3x3 array of texels with a concentration of 0.5 (See Table S3 for the minimum values). The initial concentration of the substrate s was 1.0 everywhere. All concentrations were represented with 32-bit floating point accuracy.

Supplementary Equations

To show that the results obtained for the two-substance system in Fig. 2B also hold for the three-substance system in Fig. 2A, we have constructed a simulation model corresponding directly to Fig. 2A. The equations have the form:

$$\frac{\partial[TNF\alpha]}{\partial t} = \rho_{[TNF\alpha]0} - \mu_{[TNF\alpha]}[TNF\alpha] + \eta[IL17] - k[TNF\alpha]^2[IL23] + D_{[TNF\alpha]}\nabla^2[TNF\alpha]$$

$$\frac{\partial[IL17]}{\partial t} = \rho_{[IL17]0} - \mu_{[IL17]}[IL17] + k[TNF\alpha]^2[IL23] + D_{[IL17]}\nabla^2 2[IL17]$$

$$\frac{\partial[IL23]}{\partial t} = \rho_{[IL23]0} - \mu_{[IL23]}[IL23] - k[TNF\alpha]^2[IL23] + D_{[IL23]}\nabla^2[IL23]$$

Parameter values resulting in the different pattern classes shown in Fig. 4 are collected in Table S3.

Supplementary Tables and Figures

Molecule	*MW* [kDa]	D_{tiss} [µm2/s]
TNFα	26	154.4
IL17	35	123.6
IL23	54.1	89.1

Table S1. Diffusion coefficients for the three cytokines involved in our model using the empirical formula $D_{tiss} = 1.778 \times 10^{-4} \times MW^{-0.75}$ (Swabb et al., 1974) (Equation F in their paper; MW = molecular weight), related to Figure 2. The actual rates of macromolecule transport in a tissue may differ from these estimates, as other factors may also play a role. These include convection, which may run in the direction opposite to the concentration-gradient-driven diffusion (Swabb et al., 1974), and cell proliferation, which may be relevant to the transport of cytokines otherwise mostly confined to their mother cells.

Name	Papular	Small Plaque	Large Plaque	Annular	Rosette	Reniform
$\rho_{s0}=\mu_s$	0.046	0.084	0.091	0.001	0.009	0.011
μ_a *(before treatment)*	0.116	0.141	0.148	0.028	0.056	0.057
μ_a *(during treatment)*	0.120	0.1467	0.153	0.04	0.0625	0.065
maxSteps	12,620	14,000	143,000	4,500	3,900	15,500
treatSteps	12,000	12,000	140,000	1,700	2,700	13,000

Table S2. Parameter values used to generate the six classes of psoriasis plaque patterns, related to Fig. 4. In all simulations $k = 1$, $\rho_{a0} = 0$, $D_a = 0.25$, and $D_s = 0.5$. Simulations were carried out using forward Euler methods with time step $dt = 0.4$ for *maxSteps* iterations, with the treatment starting after *treatSteps* iterations.

Name	Papular	Small Plaque	Large Plaque	Annular	Rosette	Reniform
ρ_{s0}	[0.04510, 0.04705]	[0.08375, 0.15000]	[0.09060, 0.09110]	[0.00075, 0.00285]	[0.00875, 0.00910]	[0.01085, 0.01112]
ρ_{a0}	[0.00000, 0.00075]	[0.00000, 0.00525]	[0.00000, 0.00002]	[0.00000, 0.00022]	[0.00000, 0.00015]	[0.00000, 0.00008]
μ_s	[0.04435, 0.04725]	[0.03475, 0.08475]	[0.09085, 0.09175]	[0.00000, 0.00125]	[0.00875, 0.00910]	[0.01085, 0.01120]
μ_a	[0.11265, 0.11899]	[0.10000, 0.14180]	[0.14785, 0.14870]	[0.01500, 0.03500]	[0.05360, 0.05650]	[0.05620, 0.05750]
D_s	[0.46000, 0.57500]	[0.42500, 0.80000]	[0.46100, 0.50500]	[0.00000, 1.05000]	[0.47500, 0.52500]	[0.42500, 0.61500]
D_a	[0.22000, 0.27000]	[0.17500, 0.29000]	[0.24500, 0.27000]	[0.15000, 0.75000]	[0.23500, 0.27500]	[0.22500, 0.28500]
k	[0.95900, 1.05000]	[0.98800, 1.60000]	[0.99000, 1.00200]	[0.75000, 1.35000]	[0.98500, 1.06500]	[0.97500, 1.01500]

Table S3. Ranges of parameter values resulting in pattern formation, related to Figure 4. For each varied parameter all remaining values are as in Table S2.

Pattern	A	B	C	D1	D2	D3
Minimum initial concentration of the activator at the spots	0.208	0.244	0.256	0.088	0.126	0.127

Table S4. Minimum concentrations of activator A needed to initiate the formation of patterns, related to Figure 4.

Parameter	Papular	Small Plaque	Large Plaque	Annular	Rosette	Reniform
$\mu_{[IL23]} = \rho_{[IL23]0}$	0.04	0.045	0.055	0.001	0.009	0.011
$\mu_{[TNF\alpha]}$(before treatment)	0.103	0.103	.115	0.028	0.055	0.054
$\mu_{[TNF\alpha]}$ (during treatment)	0.107	0.1087	0.12	0.04	0.0615	0.062
maxSteps	13,000	14,000	143,000	4,500	3,900	15,500
treatSteps	12,000	12,000	140,000	1,700	2,700	13,000

Table S5. Parameter values for generating the six classes of psoriasis plaque patterns using the three-substance model, related to Figure 4. In all simulations $k = 1, \eta = 2$, $\rho_{[TNF\alpha]0} = \rho_{[IL17]0} = 0$, $\mu_{[IL17]} = 1$, $D_{[IL23]} = 0.5, D_{[TNF\alpha]} = D_{[IL17]} = 0.25$. Simulations were carried out using forward Euler methods with time step $dt = 0.4$ for *maxSteps* iterations, with the treatment starting after *treatSteps* iterations.

Figure S1. Morphological details of different patterns of skin lesions in psoriasis, related to Figure 1. **A:** Psoriatic papule. Note that the scale and the thickness is accentuated in the center, indicating that the inflammatory reaction is most intense in the center of the lesion. **B:** Mature psoriasis plaque showing more activity in the periphery (open arrowheads) than in the center. **C:** Resolution of psoriatic plaques during treatment. Note central clearing of the plaque and residual peripheral activity producing a circinate pattern. **D:** Internal patterning of the plaques showing polygonal faceting. **E**: Merging circinate lesions. Annular plaques merge into polycyclic structures with clearance of the cross-sectioning parts of the lesions (open arrowhead). **F:** Reniform pattern on mucosal surface of the tongue (lingua geographica, left) and on the skin (right). Yellow solid arrows show the notched part of the lesion, black open arrowheads show the curled part at the notch.
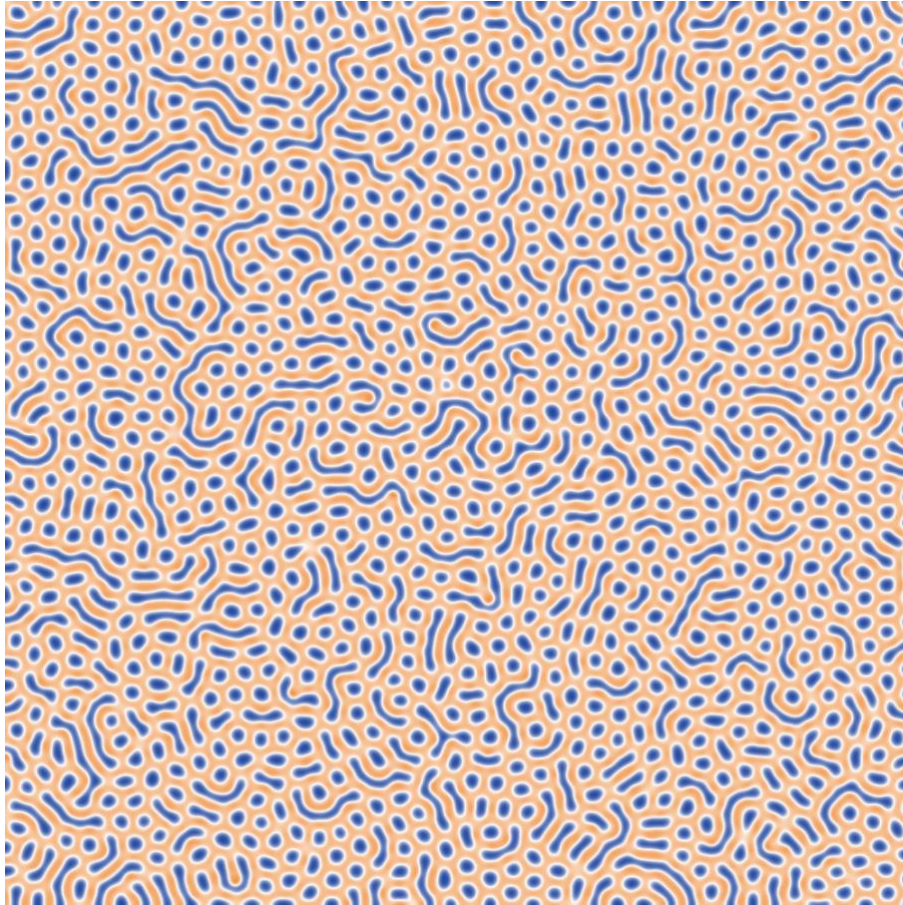
Figure S2. Example of a pattern generated de novo using the Gray-Scott model (Equation 2) after 6000 iterations, related to Figure 3. The concentration is visualized from blue to orange. Parameter values: $f = 0.042, c = 0.06, D_a = 0.25, D_s = 0.5, dt = 1$. The initial conditions are a homogenous distribution everywhere, with the addition of a small amount of noise: a=0.22557, s=0.45219±0.000001.

Supplementary Movies

Movie S1. Simulated development and response to treatment of papular lesions, related to Figure 4

Movie S2. Simulated development and response to treatment of small plaque / nummular lesions, related to Figure 4

Movie S3. Simulated development and response to treatment of large plaque lesions, related to Figure 4

Movie S4. Simulated development and response to treatment of annular lesions, related to Figure 4

Movie S5. Simulated development and response to treatment of rosette lesions, related to Figure 4

Movie S6. Simulated development and response to treatment of reniform lesions, related to Figure 4

References for Supplemental Information

Ayala, F. (2007). Clinical presentation of psoriasis. Reumatismo *59 Suppl 1*, 40–45.

Baker, H. (1971). Psoriasis--clinical features. Br. Med. J. *3*, 231–233.

Balato, N., Di Costanzo, L., and Balato, A. (2009). Differential diagnosis of psoriasis. J. Rheumatol. Suppl. *83*, 24–25.

Beylot, C., Puissant, A., Bioulac, P., Saurat, J.H., Pringuet, R., and Doutre, M.S. (1979). Particular clinical features of psoriasis in infants and chidren. Acta Derm. Venereol. Suppl. *87*, 95–97.

Buxton, P.K. (1987). ABC of Dermatology. Psoriasis. Br. Med. J. *295*, 904–906.

Champion, R.H. (1986). Psoriasis. Br. Med. J. *292*, 1693–1696.

Chau, T., Parsi, K.K., Ogawa, T., Kiuru, M., Konia, T., Li, C.-S., and Fung, M.A. (2017). Psoriasis or not? Review of 51 clinically confirmed cases reveals an expanded histopathologic spectrum of psoriasis. J. Cutan. Pathol. *44*, 1018–1026.

Christophers, E. (2001). Psoriasis--epidemiology and clinical spectrum. Clin. Exp. Dermatol. *26*, 314–320.

Cordoro, K.M. (2008). Management of childhood psoriasis. Adv. Dermatol. *24*, 125–169.

Dematté, L., and Prandi, D. (2010). GPU computing for systems biology. Brief. Bioinform. *11*, 323–333.

Di Meglio, P., Villanova, F., and Nestle, F.O. (2014). Psoriasis. Cold Spring Harb. Perspect. Med. *4*.

Fernandes, S., Pinto, G.M., and Cardoso, J. (2011). Particular clinical presentations of psoriasis in HIV patients. Int. J. STD AIDS *22*, 653–654.

Gropper, C.A. (2001). An approach to clinical dermatologic diagnosis based on morphologic reaction patterns. Clin. Cornerstone *4*, 1–14.

Harris, M.J., Coombe, G., Scheuermann, T., and Lastra, A. (2005). Physically-based visual simulation on graphics hardware. In ACM SIGGRAPH 2005 Courses on - SIGGRAPH '05.

Hernández-Vásquez, A., Molinari, L., Larrea, N., and Ciapponi, A. (2017). Psoriasis in Latin America and the Caribbean: a systematic review. J. Eur. Acad. Dermatol. Venereol. *31*, 1991–1998.

Hodge, L., and Comaish, J.S. (1977). Psoriasis: current concepts in management. Drugs *13*, 288–296.

Jablonska, S., Blaszczyk, M., and Kozlowska, A. (2000). Erythema gyratum repens-like psoriasis. Int. J. Dermatol. *39*, 695–697.

Kumar, B., Kaur, I., and Thami, G.P. (1995). Plantar psoriasis: clinical correlation of lesion pattern to weight bearing. Acta Derm. Venereol. *75*, 157–158.

Lal, S. (1966). Clinical Pattern of Psoriasis in Punjab. Indian J. Dermatol. Venereol. Leprol. *32*, 5–8.

Lebwohl, M. (2003). Psoriasis. Lancet *361*, 1197–1204.

Magro, C.M., and Crowson, A.N. (1997). The clinical and histomorphological features of pityriasis rubra pilaris. A comparative analysis with psoriasis. J. Cutan. Pathol. *24*, 416–424.

Meier, M., and Sheth, P.B. (2009). Clinical spectrum and severity of psoriasis. Curr. Probl. Dermatol. *38*, 1–20.

Melski, J.W., Bernhard, J.D., and Stern, R.S. (1983). The Koebner (isomorphic) response in psoriasis. Associations with early age at onset and multiple previous therapies. Arch. Dermatol. *119*, 655–659.

Menter, A., and Barker, J.N. (1991). Psoriasis in practice. Lancet *338*, 231–234.

M G, G., Talwar, A., Kumar B C, S., M, R., A S, N., and H B, M. (2013). A clinical and epidemiological study of psoriasis and its association with various biochemical parameters in newly diagnosed cases. J. Clin. Diagn. Res. *7*, 2901–2903.

Mitchell, J.C. (1962). The Distribution Patterns of Psoriasis: Observations on the Koebner Response. Can. Med. Assoc. J. *87*, 1271–1274.

Morris, A., Rogers, M., Fischer, G., and Williams, K. (2001). Childhood psoriasis: a clinical review of 1262 cases. Pediatr. Dermatol. *18*, 188–198.

Naldi, L., and Gambini, D. (2007). The clinical spectrum of psoriasis. Clin. Dermatol. *25*, 510–518.

de Oliveira, S.T., Maragno, L., Arnone, M., Fonseca Takahashi, M.D., and Romiti, R. (2010). Generalized pustular psoriasis in childhood. Pediatr. Dermatol. *27*, 349–354.

Picciani, B., Santos, V. de C., Teixeira-Souza, T., Izahias, L.M., Curty, Á., Avelleira, J.C., Azulay, D., Pinto, J., Carneiro, S., and Dias, E. (2017). Investigation of the clinical features of geographic tongue: unveiling its relationship with oral psoriasis. Int. J. Dermatol. *56*, 421–427.

Rasmussen, J.E. (1986). Psoriasis in children. Dermatol. Clin. *4*, 99–106.

Raychaudhuri, S.K., Maverakis, E., and Raychaudhuri, S.P. (2014). Diagnosis and classification of psoriasis. Autoimmun. Rev. *13*, 490–495.

Reich, K., Krüger, K., Mössner, R., and Augustin, M. (2009). Epidemiology and clinical pattern of psoriatic arthritis in Germany: a prospective interdisciplinary epidemiological study of 1511 patients with plaque-type psoriasis. Br. J. Dermatol. *160*, 1040–1047.

Saleh, D., and Tanner, L.S. (2018). Psoriasis, Guttate. (StatPearls Publishing).

Schön, M.P., Boehncke, W.-H., and Bröcker, E.B. (2005). Psoriasis: Clinical manifestations, pathogenesis and therapeutic perspectives. Discov. Med. *5*, 253–258.

Seneschal, J., Milpied, B., and Taieb, A. (2012). Cutaneous drug eruptions associated with the use of biologies and cutaneous drug eruptions mimicking specific skin diseases. Chem. Immunol. Allergy *97*, 203–216.

Stankier, L. (1974). Diseases of the skin. Psoriasis. Br. Med. J. *1*, 27–29.

Stern, R.S. (1997). Psoriasis. Lancet *350*, 349–353.

Swabb, E.A., Wei, J., and Gullino, P.M. (1974). Diffusion and convection in normal and neoplastic tissues. Cancer Res. *34*, 2814–2822.

Talwar, S., Tiwari, V.D., Lakhtakia, R., and Panvelkar, V. (1995). Sequential clinico-histological studies in psoriasis following methotrexate therapy. Indian J. Dermatol. Venereol. Leprol. *61*, 284–287.

Whyte, H.J., and Baughman, R.D. (1964). Acute Guttate Ppsoriasis Aand Sstreptococcal Infection. Arch. Dermatol. *89*, 350–356.

Wollenberg, A., and Eames, T. (2011). Skin diseases following a Christmas tree pattern. Clin. Dermatol. *29*, 189–194.

Ziemer, M., Eisendle, K., and Zelger, B. (2009). New concepts on erythema annulare centrifugum: a clinical reaction pattern that does not represent a specific clinicopathological entity. Br. J. Dermatol. *160*, 119–126.